Non-Inductive Improved H-Mode Operation at ASDEX Upgrade

A. Bock,[1,*] E. Fable,[1] R. Fischer,[1] M. Reich,[1] D. Rittich,[1] J. Stober,[1] M. Bernert,[1]
A. Burckhart,[1] M. Dunne,[1] B. Geiger,[1] L. Giannone,[1] V. Igochine,[1] A. Kappatou,[1]
R. McDermott,[1] A. Mlynek,[1] T. Odstrčil,[1] G. Tardini,[1] H. Zohm,[1] and the ASDEX Upgrade Team

[1]*Max-Planck-Institut für Plasmaphysik, Boltzmannstr. 2, 85748 Garching, Germany*

(Dated: 2017-03-30)

Abstract

Recent improvements to the heating and diagnostic systems on the ASDEX Upgrade tokamak allow renewed investigations into non-inductive operation scenarios with improved confinement in a full-metal device. Motivated by this, a scenario with $\beta_N \approx 2.7$, $q_{95} \approx 5.3$ and a high non-inductive current fraction $f_{NI} \gtrsim 90\%$ has been developed. The scenario offers good confinement with $H_{98}(y,2) > 1.1$ and normalised ion temperature gradients $R/L_{T_i} \approx 12$. Moreover, it is robust against resistive magnetohydrodynamic (MHD) instabilities, but does suffer from ideal MHD instability when $\beta_N \gtrsim 2.8$. To verify the understanding of the plasma transport processes, the heat transport was modelled using TGLF. This revealed that electromagnetic effects at high β and/or from fast ions appear to be missing from TGLF's physics model. As accurate reconstruction of the plasma equilibrium is crucial for studies of advanced scenarios, this publication also documents the presence of polarised background light that can contaminate Motional Stark Effect (MSE) measurements and thus interfere with equilibrium reconstruction.

*Electronic address: alexander.bock@ipp.mpg.de

I. INTRODUCTION

Operation in the high-confinement regime (H-mode) is foreseen for future tokamak-based fusion power plants due to its favourable performance. An inherent drawback of the conventional H-mode is its dependence on ohmic current induced by the central solenoid to maintain the toroidal plasma current. Moreover, at high plasma pressure the H-mode is susceptible to deleterious magnetohydrodynamic (MHD) instabilities like neoclassical tearing modes (NTMs).

Manipulation of the q-profile, for example by centrally elevating it, can alleviate these drawbacks by increasing the plasma's intrinsic bootstrap current $j_{\mathrm{bs}} \sim q$, which reduces the plasma's dependence on inductive current, and by eliminating the rational values of q required for lower-helicity NTMs. While doing so, it is important to sustain an adequate fusion performance, which requires good confinement. Heat transport in particular must be properly understood in order to predict the performance of future scenarios and devices and design them accordingly.

Different variants of so-called advanced scenarios have been investigated in a variety of machines, including JET, JT-60U, DIII-D and ASDEX Upgrade (AUG). Experiments at JET using current overshoot techniques showed transiently improved confinement although without achieving high bootstrap fractions and thus non-inductive conditions [1]. Other studies at JET using strong heating in the current rise phase of the discharge were able to transiently create strongly reversed q-profiles that lead to the formation of internal transport barriers (ITBs) [2]. Similar results were obtained at JT-60U where early heating again lead to strongly reversed q-profiles whose associated ITB sustained a transient bootstrap fraction of over 90% with excellent confinement [3]. Outstanding confinement under non-inductive conditions was also achieved at DIII-D by exploiting an anomalous current redistribution phenomenon that allows current drive efficiency to be maximised through on-axis current deposition [4, 5]. Lastly, previous investigations on AUG have also achieved non-inductive operation and good confinement as well as demonstrated that slight variations of the start-up can have a noticeable impact on the final confinement achieved [6, 7].

Recent improvements to AUG's heating and diagnostic systems [8–11] have motivated the renewed studies of advanced scenarios that are presented here. Specifically, the goal of the studies presented here was to investigate the stability and confinement properties of plasmas with centrally elevated q-profiles, and to assess their potential for extended pulse lengths. Furthermore, in contrast to the other examples mentioned above, a special focus lies on achieving the desired conditions without relying on the initial conditions. This way, the resulting plasma state is directly

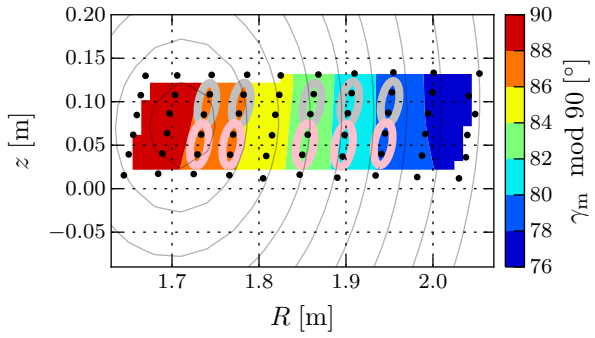

FIG. 1: Measurement locations of the conventional MSE diagnostic. Pink and silver highlighting indicate the locations of π- and σ-measurements, respectively. Grey curves show flux surfaces, colours show simulated MSE angle contours modulo 90°.

controllable without requiring precise timing of the heating scheme in the current ramp up phase of the plasma discharge. Also, since AUG has been converted into a full-tungsten machine, these new studies document the success of developing a non-inductive improved H-mode scenario in a reactor-relevant full-metal machine.

The paper is structured as follows: Section II discusses recent findings regarding the susceptibility of Motional Stark Effect (MSE) diagnostics to polarised background light and quantifies its impact on the studies of this paper. Section III presents experimental results of quasi-stationary non-inductive operation in reactor-relevant conditions [12, 13]. In section IV, the results of heat transport modelling of the non-inductive regime with TGLF are documented. A summary and outlook are given in section V.

II. ACCURACY OF EQUILIBRIUM RECONSTRUCTION

The foundation of advanced scenarios is a non-standard magnetic equilibrium, in particular a modified q-profile. Not only does it directly influence the bootstrap current density [14–16], but also the plasma transport [17–19]. As such, an accurate diagnosis of the q-profile is a prerequisite for understanding these scenarios. To that end, ASDEX Upgrade's current profile diagnostics have been expanded to include an imaging MSE system [20, 21] and a Faraday rotation polarimetry system [22] in addition to the conventional MSE [10]. The first two have been included in all equilibrium reconstructions presented in this work, which were carried out using the novel

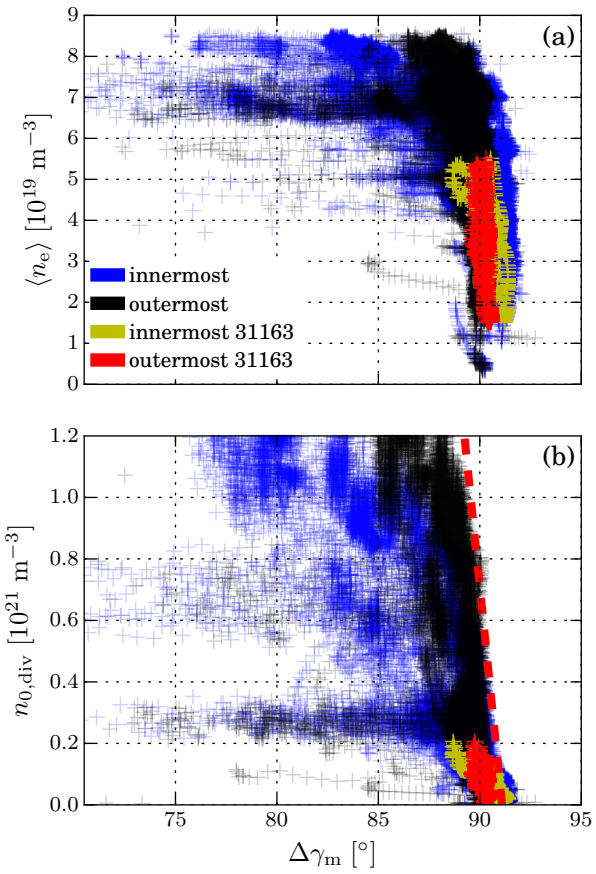

FIG. 2: Correlation between (a) line-averaged central electron density $\langle n_e \rangle$ and (b) divertor neutral density $n_{0,div}$ and MSE measurement difference between π- and σ-measurements $\Delta\gamma_m$, taken from 134 discharges. The differences for the inner- and outermost pairs of measurements (see figure 1) are shown. Data from discharge #31163 (yellow, red) represent operational space of the scenario presented in this paper.

equilibrium code IDE [11].

For the MSE measurements to be useful, they must be free of contamination from spurious signals. In recent years, however, the MSE diagnostic has been subject to drifts of the measurements. The source of the intra-discharge drifts has now been identified: they can be attributed to interference from polarised background light. This was accomplished by re-configuring the lines of sight of the MSE diagnostic to simultaneously probe both the π- and σ-emissions, whose polarisation must be perpendicular to each other. As shown in figure 1, the measurements of the five π-σ-pairs are expected to have a stable difference of about 90°. Since the measurements could not be taken at the exact same location, some small deviations from the ideal 90° difference are to be expected.

Using this set-up, a database of 134 discharges was compiled and used to determine correlations

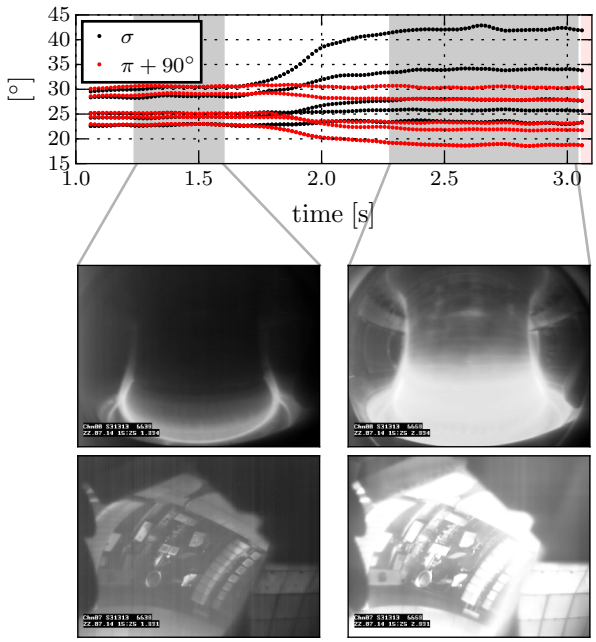

FIG. 3: MSE measurements and light emissions inside the tokamak (#31313). Severe contamination of the MSE data occurs during high emissions phases.

between the measured differences and other physical quantities. The two most striking ones are displayed in figure 2. With increasing density the measurement deteriorates significantly with drifts of up to several tens of degrees. Similarly, with increasing divertor neutral density the measurements are always compromised to some degree as no unaffected data points exist at non-zero neutral density. This is highlighted by the tilted dashed red line which shows that no clean measurement is possible for $n_{0,\mathrm{div}} > 0$. The density correlation can be explained by the beam attenuation that reduces signal towards the plasma core. This can also be seen by the varying effect on inner and outer measurements. As the intensity of the signal of interest drops, the influence of polarised background light grows. The divertor neutral flux density can be taken as a measure for the light emissions originating in the divertor, which is a principal source of polarised background light [23]. Although this light is originally unpolarised, reflections on AUG's tungsten walls will impose a partial polarisation on any light, which can then interfere with the measurement. This has been exacerbated by the conversion from carbon to tungsten since the latter has a higher reflectivity. An example of a discharge with strong light emissions is shown in figure 3. Initially, the measurements are unaffected, but as the torus brightens during a phase of high gas puff, the measurements experience strong drifts due to the increased background light.

It should be noted that the large scatter in the data indicates that other influences also effect the

fidelity of the measurements. However, no compelling correlations could be found to explain it in bulk and individual discussion of subsets of the data is beyond the scope of this publication.

In contrast to the observations on AUG, no deterioration of the measurement quality has been found on DIII-D [24], which is consistent with its lack of highly reflective metal walls. Conversely, the observations on AUG are in line with those from Alcator C-Mod [23], whose molybdenum walls cause similar interference. This lead to the development of a system to subtract the polarised background [25]. This system's design is currently being adapted for ASDEX Upgrade. As such, it was not yet available for the studies presented here.

Nevertheless, since all experiments were performed at low density to maximise current drive efficiency, the disadvantageous conditions described above (high plasma density and/or high divertor neutral flux density) were avoided. Hence, the deleterious impact of polarised background light could be kept to a minimum (cf. the red and yellow points in figure 2), resulting in a systematic error that is estimated to be of the order of 0.2°, which yields a safety factor accuracy of $\Delta q \lessapprox 0.2$ towards the plasma centre. In the presence of MHD markers like NTMs, known values of q can be used to further constrain the equilibrium reconstruction and thus validate the MSE measurements, thereby alleviating this uncertainty altogether. Note that the measurements are too coarse for an accurate reconstruction of q_0 (cf. figure 6(a)). Since the affected plasma volume is small, this has no impact on the overall results presented in the following.

III. NON-INDUCTIVE IMPROVED H-MODE SCENARIO

A. General Description

The goal of this investigation is to study discharges with centrally elevated and flattened q-profile that promise better stability against low-helicity MHD instabilities while also maximising bootstrap current. In order to be close to the parameters of future reactors, the studied discharges aim to maintain a substantial plasma current, in this case $I_\mathrm{p} = 800\,\mathrm{kA}$ with $|B_\mathrm{t}| = 2.5\,\mathrm{T}$ for $q_{95} \approx 5.3$. Additionally, to maximise both bootstrap current and external non-inductive current drive, the plasma density ($\langle n_\mathrm{e} \rangle \approx 6 \cdot 10^{19}\mathrm{m}^{-3}$) and by extension collisionality $\nu^* < 0.1$ are kept low across most of the major radius in the stationary phase. A high wall clearance is used to compensate for the lack of additional gas puffing which would normally be used in AUG to prevent the influx of impurities, but would also raise the density.

Many approaches to enter advanced scenario conditions rely on heating the plasma early in the current ramp-up phase to extend the relaxation of the initially hollow q-profile. A disadvantage of this is that during the ramp-up the plasma is hard to diagnose and all changes are very sensitive to the precise timing of the applied heating [7]. Variation of the plasma parameters in this phase is often limited to trial and error. In contrast to this, the approach presented in this paper is to use external current drive to tailor the current and thus the q-profile of an already equilibrated plasma and subsequently increase $\beta = \langle p \rangle / (B^2/2\mu_0)$ via additional NBI to increase f_{bs}. The target-β is maintained via feedback control of the NBI sources, which also allows for a controlled variation thereof to probe the plasma's stability limits.

In addition to on- and off-axis NBI, off-axis electron-cyclotron current drive (ECCD) plays a major role in shaping the q-profile. The typical configuration used in this work is shown in figure 4. Several factors played a role in choosing this specific EC deposition profile. $q_{\mathrm{min}} > 1$ is desired to eliminate periodic, sawtooth-induced confinement degradation, which requires off-axis current drive. However, the EC deposition cannot be directed too far outside because current drive efficiency strongly depends on T_{e}, which decreases with increasing minor radius, and because relatively central ECRH heating is needed to prevent central tungsten accumulation. In addition to these constraints, the Shafranov-shift at the desired β value must also be taken into account to achieve a deposition profile consistent with the other current drivers (NBI, bootstrap current) and the target q-profile.

A typical example of this scenario will be presented in the next subsection, followed by a demonstration of its independence of initial conditions and viability for extended operation. Finally, the stability properties will be documented. It should be noted that the exploitation of an anomalous flux diffusion mechanism, which would maximise current drive efficiency by allowing current drive deposition on-axis [4, 5], was not part of this scenario, but will be investigated in future studies.

B. Typical Example

Time traces from an example discharge are shown in figure 5. As explained before, no additional heating is applied during the initial current-ramp up, rather only after 1.3 s. After 2.0 s the β feedback control increases NBI heating until the target value of $\beta_{\mathrm{N}} = \beta \cdot (aB)/I_{\mathrm{p}} = 2.7$ is reached and maintained from 3.5 s to 5.0 s, which equates to about one resistive time τ_{R}. In this controlled

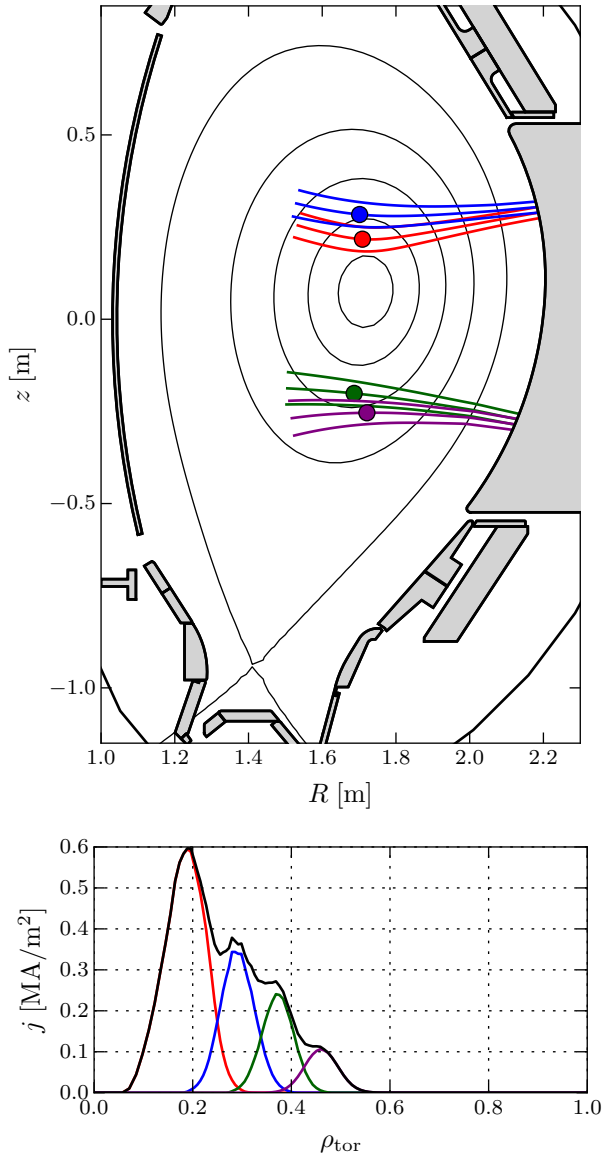

FIG. 4: Plasma shape with EC beam traces and equidistant poloidal flux surfaces, and ECCD deposition profile (#32305, 4.0 s).

phase, the loop voltage is reduced until it oscillates around zero. This shows that the induction of current by the central solenoid has ceased. The modelling of the toroidal current contributions shows that the ohmic current drops to less than 10% of the total plasma current in the stationary phase. Note that the ohmic current is calculated by subtracting all modelled non-inductive contributions from the total plasma current. Consequently, systematic deficiencies of these models may affect the balance of the different current contributions.

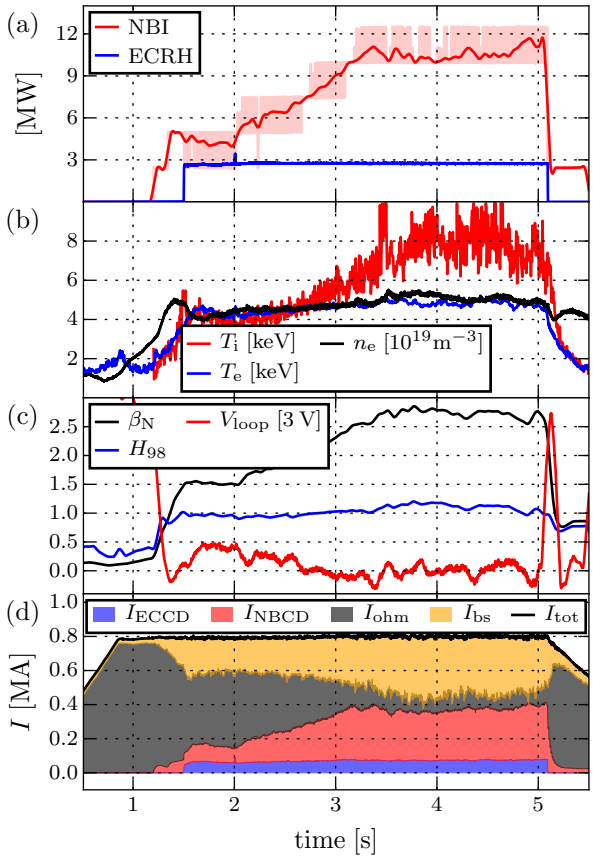

FIG. 5: (a) Heating trajectories. (b) Evolution of central temperatures and line-averaged central electron density. (c) Evolution of key plasma parameters. (d) Composition of toroidal plasma current; total current I_{tot} and bootstrap current I_{bs} as reconstructed by IDE [11], I_{ECCD} from TORBEAM [26], I_{NBCD} from TRANSP/NUBEAM [27, 28]. (#32305)

That only a small amount of inductive current remains is also supported by the reconstructed/measured current density profile j_{tot} and the modelled current density profiles shown in figure 6(b). The modelled non-inductive contributions add up to almost the total measured current density j_{tot} and do reach into its confidence band across the entire minor radius. The biggest discrepancy is near the magnetic axis. However, in this area the q-profile (cf. figure 6(a)) also exhibits the largest uncertainty. It is reconstructed with IDE using not only data from standard magnetic and pressure diagnostics, but also conventional MSE and Faraday rotation polarimetry. As mentioned before, these measurements did not extend into the very centre of the plasma (cf. section II). Thus, if q were really centrally elevated above what is obtained in the reconstruction, then not only would j_{tot} decrease near the axis, but j_{bs} would also increase, further bridging the gap between the

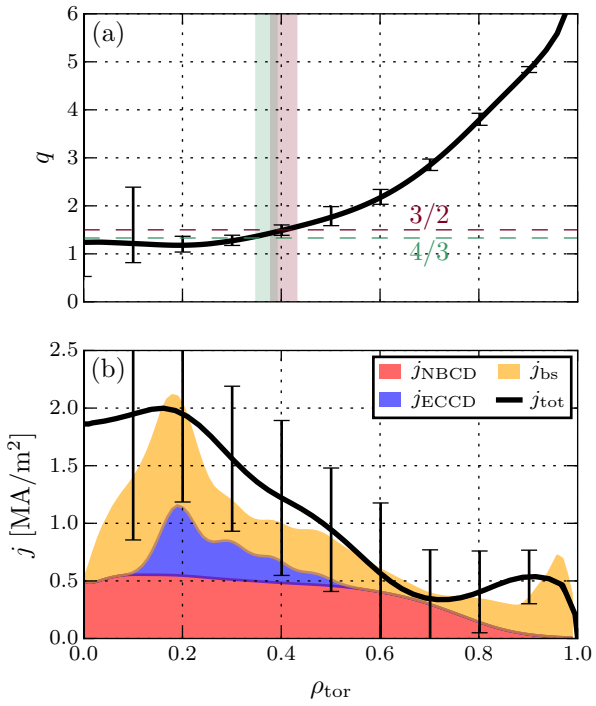

FIG. 6: Average (a) q-profile and (b) current density profiles between 4.5-5.0 s in #32305. Shaded areas in (a) indicate locations of (4/3) and (3/2) modes, derived from correlation of temperature data with magnetic measurements [29]. Coloured regions in (b) show modelled non-inductive toroidal current densities, solid black line with error bars indicates the toroidal current density profile as obtained from equilibrium reconstruction that is based on experimental data.

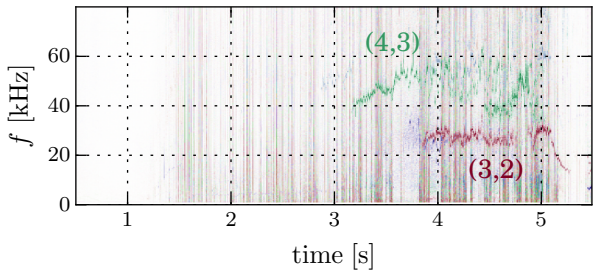

FIG. 7: Spectrogram of MHD activity in #32305.

reconstruction and the model and reducing the remaining inductive current.

In summary, the plasma can be considered to be very close to non-inductive conditions, although some uncertainty remains to be resolved.

Although q_{min} appears to be above unity, the uncertainty near the axis is large enough to allow

for a $q = 1$ surface. However, there is a distinct lack of any (1,1)-MHD activity in all discharges of this type, e.g. no sawteeth or comparable instabilities occur. Instead, small NTMs appear. Figure 7 shows a typical spectrogram where a (4,3)-mode appears early in the β-ramp. A small (3,2)-NTM appears once the target-β has been reached.

The growth of these NTMs saturates at a small size, leaving them weak and without any discernible impact on the plasma confinement. Hence, the transport analysis in section IV requires no special treatment of the NTM region. It has to be noted that this was not the case in all examples of this scenario. While most did show at least (4,3)-NTM activity, others had NTM growth until confinement was impacted. A positive side effect of this MHD activity is the ability to cross-check the q-profiles of the equilibrium reconstruction with the mode locations. This revealed good agreement between the two, suggesting that the reconstructions are accurate (cf. figure 6(a)).

However, uncontrolled NTMs may contribute to unwanted confinement degradation and require (preemptive) control and stabilisation [29]. Additional ECRH capacity for this will be available starting in the 2017 campaign of ASDEX Upgrade.

C. Independence of Initial Conditions

Figure 8 shows an example of the newly developed scenario where an additional 1.5 s of ohmic L-mode were added in the beginning. This gives the plasma ample time to equilibrate and allows the current-/q-profile to relax entirely. Consequently, all changes must be induced afterwards without making use of any initial conditions. Nevertheless, after the heating begins, the discharge evolves identically to the example in the previous subsection. Again I_{ohm} drops to <10% as β_{N} increases. The loop voltage decreases until it hovers around 0 V, while confinement stays favourable with $H_{98}(y, 2) > 1$. The major difference is that the non-inductive phase is disturbed by an ideal (2,1)-mode that rotates at about 10 kHz and grows over several tens of milliseconds. More details on this are given in subsection III E. For this scenario, the discharge control system is set to consider strong (2,1)-activity as irrecoverable and thus ends the experiment at 5.2 s as can be seen in figure 8.

In summary, this scenario is independent of the initial conditions of the discharge and can be entered at will. The difficult process of exploiting the initially hollow current profile by heating the discharge early, when the plasma is still notoriously hard to diagnose, can thus be avoided.

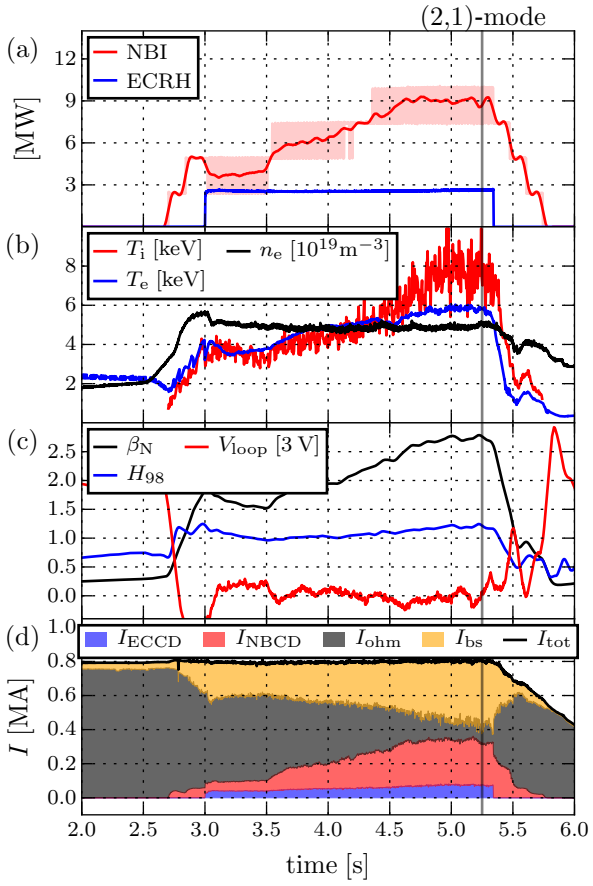

FIG. 8: (a) Heating trajectories. (b) Evolution of central temperatures and line-averaged central electron density. (c) Evolution of key plasma parameters. (d) Composition of toroidal plasma current; total current I_{tot} and bootstrap current I_{bs} as reconstructed by IDE [11], I_{ECCD} from TORBEAM [26], I_{NBCD} from TRANSP/NUBEAM [27, 28]. (#33597)

D. Extension

Time traces of an extended discharge of the same type where the current in the central solenoid I_{OH} was held constant by the discharge control system are summarised in figure 9. It follows the same programme and develops similarly to discharge #32305 (figure 5), but is extended for an additional 2 s. Specifically, between 4.5 s and 6.8 s I_{OH} is kept constant to observe the evolution of the discharge entirely without additional inductive current. Initially, the plasma current I_p jumps up briefly as the feed-forward-programmed fixed I_{OH} value was slightly underestimated and the rapid change in I_{OH} induced extra current into the plasma. This over-induced current decays quickly, after which the discharge continues to lose about 10 kA of plasma current over the next 2 s of the

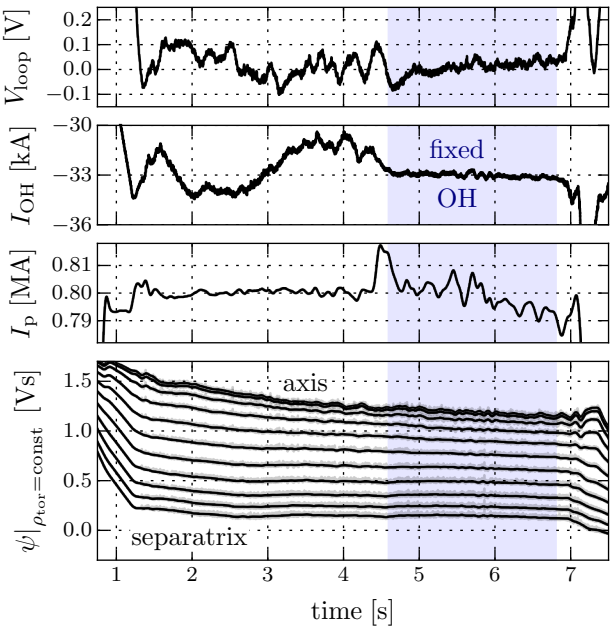

FIG. 9: Measured loop voltage V_{loop}, current in the central solenoid I_{OH}, toroidal plasma current I_{p} and poloidal flux ψ at various equidistant ρ_{tor} in #33134.

fixed-I_{OH} phase. This is equivalent to a loss of about 1.25% of I_{p}.

Also shown in figure 9 is the evolution of the poloidal flux ψ at various locations along the minor radius equidistant in ρ_{tor}. A fully non-inductive discharge would exhibit entirely flat curves as the loop voltage on a flux surface $V_{\mathrm{loop}} = \partial\psi/\partial t$ vanishes. Here ψ is approximately flat at the separatrix, which is expected as the central solenoid no longer induces current and because the bootstrap current can provide all of the required current density (cf. figure 6(b)). Closer to the axis, however, the plasma still evolves noticeably, which is consistent with a continuing decay of the remaining induced current density there. It is unclear whether the evolution would have reached a steady state in which the equilibrium and kinetic profiles are consistent with each other without requiring inductive current to maintain adequate confinement. It may be possible to optimise and shorten the heating ramp as well as exhaust AUG's maximum discharge length (< 10 s) to observe the continued evolution.

Note that the discharge shown here did incur a $(3, 2)$-NTM at about 4.45 s. Before its appearance, the global energy confinement time scaling factor $H_{98}(y, 2)$ oscillated around 1.15, then briefly rose above 1.25 before collapsing to 0.95 as the mode grew and degraded the confinement. The discharge control system responded by adding another neutral beam source to maintain the

target-β, allowing the discharge to continue with reduced confinement but otherwise unperturbed. More details about the stability properties are given in the following subsection.

E. Stability

Ultimately the cause for the appearance of the ideal mode in #33597 (cf. subsection III C) is a brief increase of β_N up to almost 2.9, despite the control system aiming for a lower value. In fact, oscillations of the plasma pressure and thus β are visible in most discharges of this scenario and every irrecoverable instability can be traced back to a sudden increase in plasma confinement that causes β_N to increase past $\sim$ 2.8. Consequently, ideal or resistive instabilities appear and cause strong confinement degradation from which the discharge cannot recover.

Conversely, as long as the discharge remains under the limit, no strong instability is observed. While NTMs appear often, they generally remain small and do not have an unacceptably strong negative impact on the discharge, seeing as the plasma maintains $H_{98}(y, 2) > 1$. When they do grow to noticeable sizes, e.g. in #33134 (cf. previous subsection), they can also be connected to brief, transient confinement improvements as above.

The sudden increases in β may be because the scenario, as will be discussed in the next section, exhibits good heat confinement properties, likely due to high values of β and/or high fast ion density as well as favourable $T_i > T_e$ in the centre (cf. figure 14(a)). Once the improved confinement sets in, the control system must respond by reducing the NBI heating power in order to maintain the target-β. This in turn reduces the fast ion population and the ion heating that maintains the temperature ratio T_e/T_i, which leads to a central confinement degradation, prompting the control system to increase heating again. If the feedback control does not respond in time, then the discharge can exceed the stability limit and incur strong MHD activity.

A further contribution to these oscillations comes from intermittent radiative losses due to tungsten, whose origin is not entirely understood, but which does again require the control system to respond. This was particularly noticeable in the case of #33134. As mentioned before, a potential intermittent tungsten influx from the wall cannot be mitigated by increasing gas puffs since the density is purposely kept low to maximise bootstrap current and external current drive efficiency.

It has to be stressed that slight local variations of the current density profile can have a decisive impact on the discharge stability, even if global parameters like normalised pressure β_N [30] and/or internal inductance l_i [31] are identical [32]. Discharge #33597 experienced an ideal mode, which

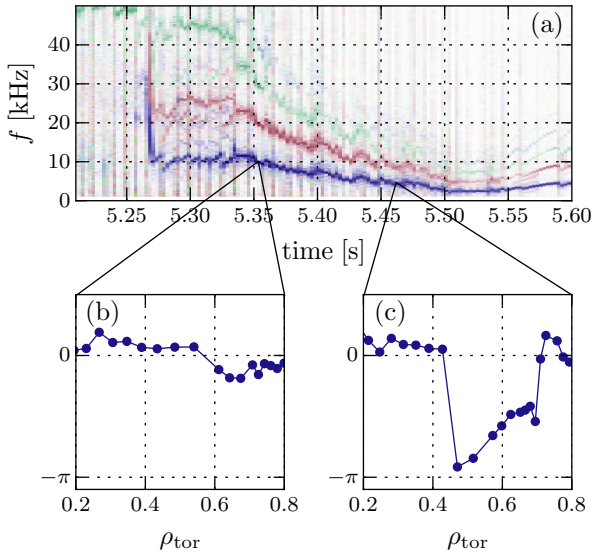

FIG. 10: (a) Spectrogram of MHD activity in #33597 and (b/c) phase of electron temperature fluctuations across minor radius at the frequency of the (2,1)-mode. Initially, the fluctuations exhibit no phase jump, i.e. the flux surfaces are deformed ideally. Later on, a phase jump of π is apparent, which means that flux surfaces have reconnected and formed magnetic islands.

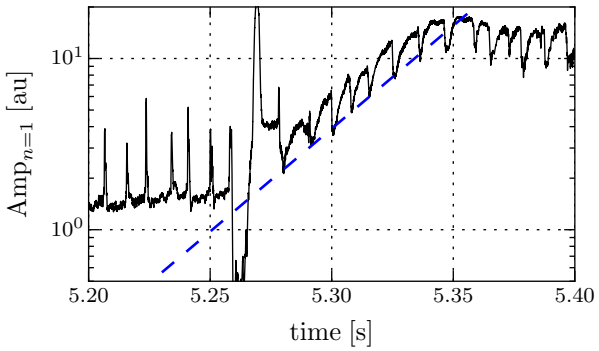

FIG. 11: Amplitude of $n = 1$ MHD-activity. The diagonal dashed blue line shows the growth of the mode ($\gamma \approx 28\ \mathrm{s}^{-1}$).

changed into a tearing mode within several tens of milliseconds, as can be seen in figure 10. Its initial growth takes place on a similar time scale as shown in figure 11. This is in line with previously observed instabilities in high-β advanced scenario discharges in JET [33] as well as NSTX [34], which also started out as ideal modes that later turned into tearing modes.

In contrast, #32305 remained stable despite the fact that it also intermittently reached up to

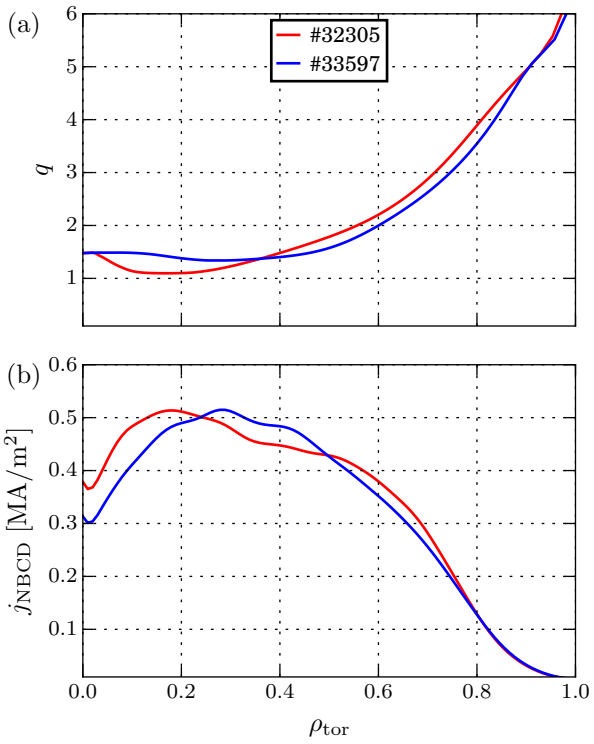

FIG. 12: (a) q-profiles and (b) neutral beam current drive as calculated by TRANSP in #32305 and #33597 at 2.5 s after first NBI source, i.e. at 3.7 s and 5.2 s, respectively.

$\beta_{\mathrm{N}} = 2.9$ and both had $l_{\mathrm{i,32305}} = l_{\mathrm{i,33597}} = 1.0$. The difference between the two, besides one being delayed, is a small difference in the NBI configuration. In discharge #33597 one of #32305's on-axis sources was swapped for an off-axis one, resulting in a slightly different NBCD profile and thus a slightly changed q-profile. This is shown in figure 12. The q-profile of #33597, being flat and elevated in the centre, is more prone to instability than its more conventional counterpart from #32305, which is consistent with previously calculated stability limits [32, 35].

In summary, stability-wise the scenario can be judged as robust as long as high β_{N} (> 2.7) is avoided. In this sense, further optimisations to the control scheme are necessary to consistently prevent overshooting this limit. Conversely, additional optimisation of the q-profile and a correction of the intrinsic error field may allow a slight increase of the limit. Significant improvements are to be expected from adding if not an entire conducting wall then at least select conductive structures close to the plasma surface which would push the limit closer towards $\beta_{\mathrm{N,ideal-wall}}$ [32, 35].

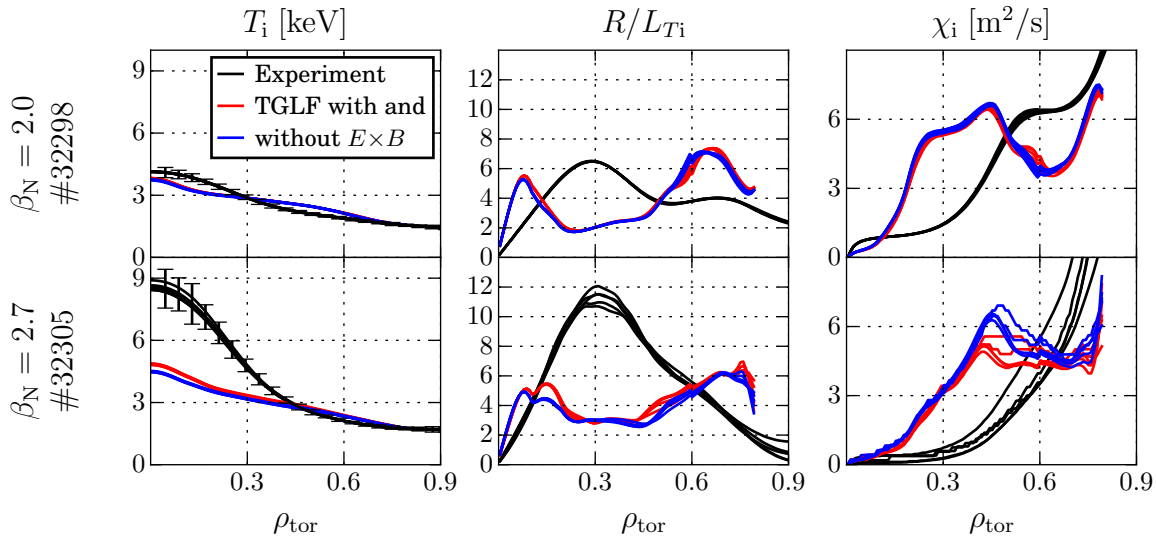

FIG. 13: Ion temperature profile, normalised ion temperature gradient and ion heat diffusivity for #32298 and #32305. The experimentally observed profiles are shown in black, and the profiles modelled with TGLF in red and blue with and without $E\times B$-effects, respectively. Curves correspond to last energy confinement time τ_R out of 500 ms of the stationary phase.

IV. TRANSPORT MODELLING WITH TGLF

While it is preferable to operate a tokamak non-inductively, its performance is ultimately the decisive characteristic. The plasma heat transport in particular must be understood in order to be able to accurately predict the performance of a future fusion power plant. Moreover, as sketched in the previous section, understanding the heat transport can help maintain a discharge as close as possible to its stability limit, and thus at maximum performance, without actually crossing it.

In previous investigations the plasma transport has been successfully modelled using TGLF [36, 37], for instance in a non-inductive H-mode scenario in DIII-D [5] or for H-modes with varying heating mixes in ASDEX Upgrade [38]. Consequently, the same approach was taken to model the heat transport in the plasma scenario presented here.

Like in [38], TGLF was embedded in the framework software ASTRA [39, 40] and calculated electron and ion heat transport coefficients with which the temperature profiles were evolved self-consistently, starting with the experimental observation as the initial conditions. Input power was calculated by TORBEAM for ECRH and TRANSP/NUBEAM for NBI. Radiative losses were tomographically reconstructed from bolometric measurements [41, 42].

The experimental temperature profiles are used as a boundary condition at $\rho_{\mathrm{tor}} = 0.8$ and evolved over 500 ms during which the discharge is kept stable, e.g. from 3.5 s to 4.5 s in #32305. This amounts to several energy confinement times $\tau_{\mathrm{E}} \approx 70$ ms, which is sufficient to reach a steady state.

Initial results showed that it was not possible to reproduce the full electron and ion temperature profiles. Especially during the $\beta_{\mathrm{N}} = 2.7$ phase of #32305, the predicted temperatures were consistently lower by about 30%. This is why subsequent analyses focussed on the ion temperature in particular, which was identified to be the main cause of the discrepancy.

The results of these analyses are summarised in figure 13 for a low-β case ($\beta_{\mathrm{N}} = 2.0$ in #32298) and a high-β case ($\beta_{\mathrm{N}} = 2.7$ in #32305). The discharges differ primarily in the applied amount of NBI power, but slight differences also occur in the equilibrium.

As a reference, figure 13 includes the respective power balance results that TGLF's calculations should match. In the low-β case, this is achieved. The χ_{i} given by TGLF is not identical to its power balance counterpart, which causes the resulting normalised ion temperature gradient $R/L_{T_{\mathrm{i}}}$ to differ qualitatively from the experimentally observed gradient. Nevertheless, the resulting T_{i} profile matches the experiment fairly well. The on-axis temperature in particular is matched within a few hundred eV, i.e. within the error bars of the experimental profile. Across the minor radius, the profile shape differs slightly and causes deviations beyond the experimental error bars. It might be tempting to frame the qualitative differences between the TGLF prediction for χ_{i} and the experimental one as evidence of a significant gap in TGLF's physics model. This, however, would neglect all other sources of uncertainty that affect this investigation. For one, the error bars on the experimental T_{i}-profile result in even larger error bars on its gradient. Consequently, the error bars on the experimental χ_{i}-profile, which also depends on the accuracy of the heat deposition modelling, are even larger. On top of this, errors of the TGLF input parameters may also affect its result. Thus, because the error bars on these derived quantities are too large, the deciding factor in judging the result must be whether the predicted temperature profile matches the experimentally observed profile — which it does.

The reproduction is not achieved in the high-β case. Here the power balance analysis shows that χ_{i} has dropped significantly inside of $\rho_{\mathrm{tor}} \approx 0.65$, resulting in almost double the $R/L_{T_{\mathrm{i}}}$. Consequently, T_{i} is now significantly higher inside of mid-radius, with a peak value on-axis of almost 9 keV. In contrast, the TGLF result is qualitatively unchanged from the low-β one and thus fails to reproduce the increased confinement. This result does not depend on $E{\times}B$-stabilisation of tur-

bulence [43] as can be understood from the fact that disabling this mechanism only appears to have a substantial effect at mid-radius for the high-β case, which is still insufficient to explain the experimental observations.

With turbulent transport being highly non-linear and TGLF employing a quasi-linear model, it is conceivable that a slight variation of the (other) input parameters might resolve this discrepancy. This turned out not to be the case. TGLF does respond to variations of, for example, the normalised magnetic shear s and/or q, the ion heating power, $T_\mathrm{e}/T_\mathrm{i}$ or even the fast ion content. However, no reasonable variation is sufficient to increase confinement as much as needed. For instance, only an increase of the ion heating by 50% (i.e. an additional two NBI sources) would allow $T_\mathrm{i}(0)$ to reach the experimental value, with the profile shape still not matching the experimental profile.

This result is seemingly contradictory to previous results from AUG [38] where both T_i and T_e were successfully reproduced by TGLF, both at lower $\beta_\mathrm{N} \approx 1.7$ and higher $\beta_\mathrm{N} \approx 2.9$. Here, the low-$\beta$ case is also reproduced, while the high-β case is not. The main difference is that while the low-β case was comparable in both examples, i.e. stationary, the high-β case in [38] was only reached briefly by rapidly doubling the NBI power from 5 MW to 10 MW and performing the calculation when the plasma reached peak stored energy. It is possible that the physics differs between such transient states and stationary phases like the ones presented in this paper. To resolve this, it may be necessary to perform further experiments where the heating scheme is varied between gradual and sudden increases of ion heating.

A potential explanation for the discrepancy in the stationary high-β phase is given by [46, 47]. There, full gyrokinetic simulations of JET discharges were performed with the GENE code [48, 49]. It was found that taking into account electromagnetic effects from fast ions as well as thermal β can substantially increase R/L_{T_i}, resulting in an increase of $T_\mathrm{i}(0)$ by several tens of percent. The physics underlying this result are not yet entirely understood, but it may also play a role in the confinement observed in #32305: β is about 35% higher than in #32298 while the fast ion density increases by up to 20% inside of mid-radius as shown in figure 14(b). Overall the fast ion population contributes about a third of the total plasma pressure, and can therefore not be neglected. It has to be stressed that TGLF does respond to changes in the fast ion density as well as the β-induced Shafranov shift. However, these changes are insufficient to account for the observed confinement.

In summary, it can be concluded that TGLF's physics model is missing key components that become relevant at high-β and/or when high fast ion densities are present. Further investigations

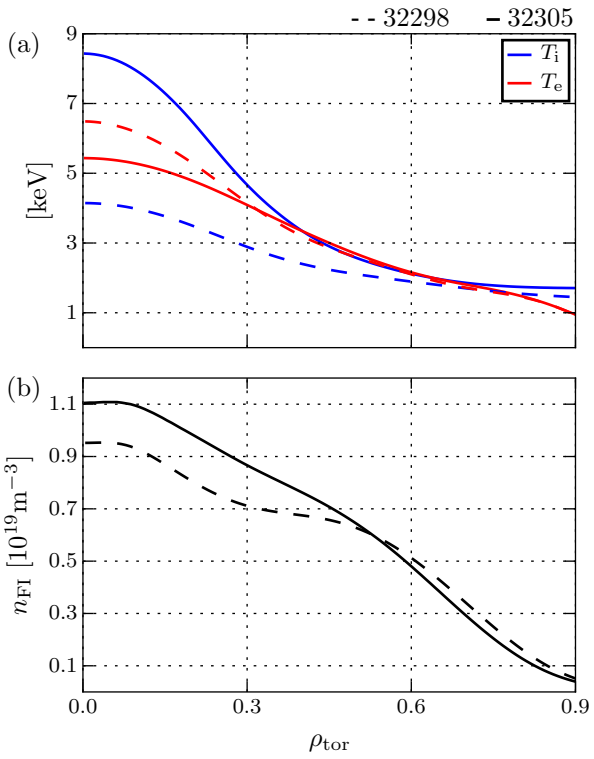

FIG. 14: (a) Ion and electron temperatures and (b) fast ion density in #32298 and #32305 at 4.0 s (dashed and solid lines, respectively). T_i is taken from charge exchange spectroscopy [44], T_e from IDA reconstruction [45], and fast ion density from TRANSP/NUBEAM [27, 28].

into this using full gyro-kinetic codes like GENE or GYRO [50] (from which TGLF is derived) may identify the missing physics to be added to TGLF. The first results of modelling these experimental observations with GENE suggest that both electromagnetic physics and fast ion effects play a crucial role in explaining the confinement properties [51].

V. SUMMARY AND OUTLOOK

A non-inductive improved H-mode scenario with $q_{95} \approx 5.3$ and $\beta_N = 2.7$ has been presented. It offers favourable confinement with $1.1 < H_{98}(y,2) < 1.2$ and reasonable stability for $\beta_N < 2.8$, and is independent of the initial conditions. Above $\beta_N \approx 2.8$, ideal and resistive MHD instabilities appear. Further ECRH capacity that will be available starting with the 2017 campaign may help stabilise resistive instabilities. Ideal instabilities may be partially stabilised by correcting the intrinsic error field of the device. Moreover, improvements to the conductivity of the vessel wall

are being investigated as a means to create a quasi-conducting wall. Modifications of the wall are not expected in the short term, which is why investigations aimed at varying and optimising the q-profile are planned. Going forward, these efforts will be directed at evolving the scenario towards a potential DEMO steady state scenario with $q_{95} \approx 4.5$ and $\beta_N = 3.5$.

In order to verify the understanding of the plasma energy confinement, the plasma heat transport was modelled using TGLF. The mechanism behind the favourable confinement quality could not be identified since the observed transport was not reproducible with TGLF. A potential explanation due to electromagnetic effects of β and/or fast ions is currently under investigation using full gyrokinetic simulations with the GENE code.

The presence of deleterious polarised background light that interferes with conventional MSE measurements has been confirmed in the ASDEX Upgrade tokamak. This light is reflected into the MSE view by the metal walls and also incurs a polarisation through these reflections. It affects the majority of discharges and is particularly strong when the plasma density and/or the divertor neutral flux density are/is high. The former results in a reduced signal due to neutral beam attenuation, while the latter creates more background light. A mitigation polychromator-system based on a design from Alcator C-Mod is being installed to compensate for the background light, but was not available for the work presented here.

---

[1] J. Hobirk *et al.*, Plasma Physics and Controlled Fusion **54**, 095001 (2012).

[2] E. Joffrin *et al.*, Plasma Physics and Controlled Fusion **44**, 1739 (2002).

[3] Y. Sakamoto *et al.*, Nuclear Fusion **49**, 095017 (2009).

[4] F. Turco *et al.*, Physics of Plasmas **22**, 056113 (2015).

[5] C. Petty *et al.*, Nuclear Fusion **56**, 016016 (2016).

[6] J. Hobirk *et al.*, Physical Review Letters **87**, 085002 (2001).

[7] J. Stober *et al.*, Nuclear Fusion **47**, 728 (2007).

[8] A. Stäbler, J. Hobirk, F. Leuterer, and F. Meo, Fusion Science and Technology **44**, (2003).

[9] D. Wagner *et al.*, IEEE Transactions on Plasma Science **36**, 324 (2008).

[10] R. C. Wolf *et al.*, Journal of Instrumentation **10**, P10008 (2015).

[11] R. Fischer *et al.*, Fusion Science and Technology **69**, 526 (2016).

[12] H. Zohm *et al.*, Nuclear Fusion **53**, 073019 (2013).

[13] H. Zohm *et al.*, in *43rd EPS Conference on Plasma Physics* (European Physical Society, Leuven, 2016).

[14] O. Sauter, C. Angioni, and Y. R. Lin-Liu, Physics of Plasmas **6**, 2834 (1999).

[15] C. Kessel, Nuclear Fusion **34**, 1221 (2002).

[16] R. Hager and C. S. Chang, Physics of Plasmas **23**, (2016).

[17] S. C. Guo and F. Romanelli, Physics of Fluids B: Plasma Physics **5**, 520 (1993).

[18] F. Jenko, W. Dorland, and G. W. Hammett, Physics of Plasmas **8**, 4096 (2001).

[19] A. G. Peeters *et al.*, Physics of Plasmas **12**, 022505 (2005).

[20] O. P. Ford, J. Howard, and R. C. Wolf, Review of Scientific Instruments **86**, 0 (2015).

[21] O. P. Ford *et al.*, The Review of scientific instruments **87**, 11E537 (2016).

[22] A. Mlynek *et al.*, in *21st Topical Conference on High Temperature Plasma Diagnostics (HTPD 2016)* (University of Wisconsin, Madison, 2016).

[23] R. T. Mumgaard, Ph.D. thesis, Massachusetts Institute of Technology, 2015.

[24] B. S. Victor *et al.*, **126**, (2016).

[25] R. T. Mumgaard, S. D. Scott, and M. Khoury, Review of Scientific Instruments **87**, 11E527 (2016).

[26] E. Poli, A. G. Peeters, and G. V. Pereverzev, Computer Physics Communications **136**, 90 (2001).

[27] TRANSP home page, http://w3.pppl.gov/transp.

[28] A. Pankin *et al.*, Computer Physics Communications **159**, 157 (2004).

[29] M. Reich, A. Bock, M. Maraschek, and ASDEX Upgrade Team, Fusion Science and Technology **61**, 309 (2012).

[30] F. Troyon *et al.*, Plasma Physics and Controlled Fusion **26**, 209 (2002).

[31] E. J. Strait, Physics of Plasmas **1**, 1415 (1994).

[32] V. Igochine, Nuclear Fusion **52**, 074010 (2012).

[33] P. Buratti *et al.*, Nuclear Fusion **52**, 023006 (2012).

[34] S. Sabbagh *et al.*, Nuclear Fusion **50**, 025020 (2010).

[35] V. Igochine, *Active Control of Magneto- hydrodynamic Instabilities in Hot Plasmas* (Springer-Verlag, Berlin/Heidelberg, 2015).

[36] G. M. Staebler, J. E. Kinsey, and R. E. Waltz, Physics of Plasmas **12**, 1 (2005).

[37] G. M. Staebler, J. E. Kinsey, and R. E. Waltz, Physics of Plasmas **14**, 055909 (2007).

[38] F. Sommer *et al.*, Nuclear Fusion **55**, 033006 (2015).

[39] G. V. Pereverzev and P. N. Yushmanov, (2002).

[40] E. Fable *et al.*, Plasma Physics and Controlled Fusion **55**, (2013).

[41] M. Bernert, Ph.D. thesis, Ludwig-Maximilians-Universität München, 2013.

[42] M. Bernert *et al.*, Review of Scientific Instruments **85**, (2014).

[43] K. H. Burrell, Physics of Plasmas **4**, 1499 (1997).

[44] E. Viezzer, T. Pütterich, R. Dux, and R. M. McDermott, Review of Scientific Instruments **83**, 103501 (2012).

[45] R. Fischer *et al.*, Fusion Science and Technology **58**, 675 (2010).

[46] J. Citrin *et al.*, Physical Review Letters **111**, 155001 (2013).

[47] J. Citrin *et al.*, Plasma Physics and Controlled Fusion **57**, 014032 (2015).

[48] F. Jenko, W. Dorland, M. Kotschenreuther, and B. N. Rogers, Physics of Plasmas **7**, 1904 (2000).

[49] T. Görler *et al.*, Journal of Computational Physics **230**, 7053 (2011).

[50] J. Candy and R. E. Waltz, Journal of Computational Physics **186**, 545 (2003).

[51] H. Doerk, tbd **tbd**, tbd (2017).